A novel approach for segmenting and mapping of local fiber orientation of continuous fiber-reinforced composite laminates based on volumetric images

Ludwig Schöttl, Dominik Dörr, Pascal Pinter, Kay A. Weidenmann, Peter Elsner, Luise Kärger

Angaben zur Veröffentlichung / Publication details:

Schöttl, Ludwig, Dominik Dörr, Pascal Pinter, Kay A. Weidenmann, Peter Elsner, and Luise Kärger. 2020. "A novel approach for segmenting and mapping of local fiber orientation of continuous fiber-reinforced composite laminates based on volumetric images." *NDT & E International* 110: 102194. https://doi.org/10.1016/j.ndteint.2019.102194.

A novel approach for segmenting and mapping of local fiber orientation of continuous fiber-reinforced composite laminates based on volumetric images

Ludwig Schöttl [a,b,*], Dominik Dörr [a], Pascal Pinter [b], Kay André Weidenmann [c], Peter Elsner [b,d], Luise Kärger [a]

[a] FAST, Karlsruhe Institute of Technology, Karlsruhe, Germany
[b] IAM-WK, Karlsruhe Institute of Technology, Karlsruhe, Germany
[c] MRM, University of Augsburg, Augsburg, Germany
[d] ICT, Fraunhofer Institute, Pfinztal, Germany

1. Introduction

1.1. Motivation

Mass reduction of components offers a lot potential to save energy. Especially in transport industries like automotive and aircraft systems, mass reduction of components is an important aspect. Therefore, enormous effort is required to create new lightweight materials and designs. Due to its high stiffness and low density, continuous fiber-reinforced polymer (CoFRP) gained enormous relevance in modern lightweight designs (cf. [1,2]).

In the last decades, computed tomography (CT) became one of the most common non-destructive testing methods in material science [3]. Modern CT systems offer the opportunity to obtain volumetric images of microstructures in a non-destructive way. Recent developments lead to higher resolution, which allows investigating structures even more detailed. Furthermore, modern laminography systems enable to investigate also larger planar parts in a non-destructive manner. Independent of the data acquisition, volumetric image analyses for micro structure quantification of composite material is a fast growing application area.

In general, there are two ways to determine the fiber orientation from volumetric images. One common approach is to segment every single fiber within the dataset and calculate its center line. This method does also enable for fiber length measurements, but a high image quality and resolution is needed. Hence, the samples have to be very small, due to the X-ray cone-beam geometry of the CT. Since a representative

* Corresponding author., FAST, Karlsruhe Institute of Technology, Karlsruhe, Germany.
E-mail address: ludwig.schoettl@kit.edu (L. Schöttl).

volume element for carbon fiber layups is rather large, a more robust method is needed for the present application, which leads to the second approach for orientation analysis. The authors [4–6] show that fiber orientations can be determined reliably with only a significant gray value gradient between fiber and matrix. As a result, single fibers do not have to be segmented individually. The result of those methods is a local principal orientation for each volume element of the entire composite. With sufficient image resolution, this approach can also be applied to segmented fibers. This provides a very robust orientation analysis and allows additionally to determine a fiber volume fraction.

The fist approach is for example applied by authors Emerson et al. [7], who implemented an image processing method to segment individual fibers of unidirectional composite materials. A method for fiber tracking and determining of fiber length distributions using CT-data is introduced by Pinter et al. [8].

Another interesting application of CT volumetric images of composite laminates are the measurement of fiber misalignment by Nguyen et al. [9], where the mid-layer volume of each laminate layer is selected manually and the influence of different manufacturing processes is investigated. Synchrotron micro-tomography acquired images are used by Requena et al. [10] for orientation distribution qualification of both, continuous carbon fiber reinforced aluminum and polymers. Besides unidirectional composites, CT characterization of fiber orientation is also used for discontinuous composites. The authors Schladitz et al. [11] used volumetric images to characterize the fiber orientation of sheet molding compounds (SMC). In the contribution of Pinter et al. [6] different methods for determining the local fiber orientation on the voxel-level based on volumetric images are compared and the method based on the structure tensor (cf. Krause et al. [12]) found out to work best in most applications.

Within this contribution, volumetric image segmentation is used to identify and separate particular regions of the image. For segmentation, a wide range of different approaches for specific application are available. Especially in medical image analysis [13,14], where parts of the skull or brain are segmented in CT or MRT data. Most of these methods are use different gray value based approaches, such as simple thresholding or region growing. Besides medical image analysis, there is also a wide range of various methods for segmenting objects in material science. For example there are segmentation methods to detect and segment damaged regions within composites [15].

The presented paper focuses on analyzing unidirectional continuous fiber-reinforced thermoplastic tape laminates. These laminates consist of several unidirectional fibers reinforcement layers with an individual orientation of each layer. Components made of UD-tapes are manufactured by tape laying and subsequent thermoforming [16]. The initial material is preimpregnated unidirectional fiber tapes, which are stacked on a planar table with a certain orientation. By adjusting the tape alignment during the stacking step, stiffness and other mechanical properties of the final component are adjusted. Subsequently, the stack is pre-consolidated and thermoformed. During the forming process step, the local fiber orientation of the laminate layers changes significantly. For designing of UD-tape components, information of the fiber orientation within the final component is essential and methods for predicting and characterizing of fiber orientations are needed.

To the author's knowledge there is so far no CT based method available to automatically separate the individual laminate layers by orientation. Volume Graphics GmbH holds a patent for a similar method [17], but did not release it in their software yet. After orientation based segmentation, the individual fiber orientation of each layer is mapped to a finite element mesh.

1.2. Theoretical principles

The most general way to describe a fiber orientation condition, is given by the distribution function $\psi(\boldsymbol{p})$ [18], where $\psi(\boldsymbol{p})$ returns a proportion value of fibers aligned in the related direction of unit vector $\boldsymbol{p}$. An alternative formulation besides the distribution function $\psi(\boldsymbol{p})$ are the orientation tensors defined by Advani and Tucker and Kanatani [18,19]. For instance the analytical second-order orientation tensor is given by

$$\boldsymbol{N} = \oint \boldsymbol{p} \otimes \boldsymbol{p} \psi(\boldsymbol{p}) \mathrm{d}\boldsymbol{p}. \tag{1}$$

In practice the distribution function ψ is usually not available. However, based on N detected fiber vectors $\boldsymbol{n}_i$, the second-order orientation tensor $\boldsymbol{N}$ is empirically given by

$$\boldsymbol{N} = \frac{1}{N} \sum_{i=1}^{N} \boldsymbol{n}_i \otimes \boldsymbol{n}_i. \tag{2}$$

Based on the empirical second-order orientation tensor $\boldsymbol{N}$, a smoothed distribution function ψ is calculated by $\psi(\boldsymbol{p}) \approx \frac{1}{4\pi} + \frac{15}{8\pi} \boldsymbol{B}\boldsymbol{F}(\boldsymbol{p})$, where $\boldsymbol{B} = \boldsymbol{N} - \frac{1}{3}\boldsymbol{I}$, $\boldsymbol{F}(\boldsymbol{p}) = \boldsymbol{p} \otimes \boldsymbol{p} - \frac{1}{3}\boldsymbol{I}$ and $\boldsymbol{I}$ represents the identity tensor, [18]. The second-order orientation tensor is symmetric ($\boldsymbol{N} = \boldsymbol{N}^T$) and due to the normalization condition ($||\boldsymbol{n}|| = 1$), the first principal moment of $\boldsymbol{N}$ is also normalized ($\mathrm{tr}(\boldsymbol{N}) = 1$).

The normalized eigenvectors $\boldsymbol{v}$ of the orientation tensor $\boldsymbol{N}$ mark the principal direction of the fiber alignment and the related eigenvalues λ represent the statistic proportion of fibers aligned in the corresponding direction [20]. All eigenvalues are sorted in the way that $\lambda_1 > \lambda_2 > \lambda_3$. Therefore, the eigenvector $\boldsymbol{v}_1$ represents the most relevant fiber orientation. In case of planar fiber alignment, the third eigenvalue λ_3 is almost zero. Based on the eigenvalues λ_1 and λ_2, the coherence value c_w of $\boldsymbol{N}$ [21] is defined by

$$c_w = \left(\frac{\lambda_1 - \lambda_2}{\lambda_1 + \lambda_2} \right)^2. \tag{3}$$

In this contribution, the coherence value c_w represents the coherence of the second-order fiber orientation tensor $\boldsymbol{N}$ and indicates the degree of fiber isotropy. If all detected fibers are perfectly aligned in one direction, c_w becomes 1. In case of planar symmetric fiber distribution, λ_1 and λ_2 are equal and the coherence value becomes zero.

2. Methods for layer segmentation and mapping

2.1. Preliminary

The gray value volumetric images used in this contribution are acquired from µCT. First the local fiber orientation of each separated fiber voxel is determined by using the structure tensor based approach (cf. Krause et al. [12] and Pinter et al. [6]). The local fiber orientations per volume element are returned as normalized fiber vectors $\boldsymbol{n}_i$.

The goal of the presented approach is to determine the local fiber orientation of all individual laminate layers at specific analyzed points. The analyzed points can be defined manually or e.g. be given by the Gaussian points of a corresponding finite element mesh.

2.2. Proceed overview

As introduced, in this manuscript shell-shaped continuous fiber-reinforced composites are investigated. First, the direction orthogonal to the local laminate layers is determined by using the fiber vectors $\boldsymbol{n}_i$ around the analyzed point. Subsequently, a local coordinate system and a cylindrical volume around each analyzed point, aligned along the normal direction is defined. The segmentation step represents the key step of the presented approach. The laminate layers within the local cylindrical volume are segmented. Finally, the local fiber orientation of each layer is determined and mapped to a FE mesh.

2.3. Normal direction $\boldsymbol{e}_{z'}$

The local shell normal direction $\boldsymbol{e}_{z'}$ is defined as the local direction orthogonal to the laminate layers (cf. Fig. 1). A is defined as a volume

around the analyzed point including several laminate layers (cf. black rectangle in Fig. 1 (a)). If A is sufficiently small, all fibers within A and consequently, all fiber vectors $\boldsymbol{n}$ within A are planar aligned.

The second-order orientation tensor calculated by using fiber vectors $\boldsymbol{n}$ within A yields two significantly bigger eigenvalues compared to the third one ($\lambda_1 > \lambda_2 \gg \lambda_3$). The first and second corresponding eigenvectors are aligned along the laminate layer plane. Following the orthogonality of symmetric tensors, the third eigenvector $\boldsymbol{v}_3$ is aligned in the normal plane direction and orthogonal to the local laminate layers. At each analyzed point, a new local coordinate system is defined in the way that $\boldsymbol{e}_{z'} = \boldsymbol{v}_3$ is oriented in shell normal direction.

2.4. Defining local considered volume B

Volume B is defined as cylindrical volume around an analyzed points with center axis aligned in $\boldsymbol{e}_{z'}$-direction and radius R. Fig. 2 illustrates the principal shape and orientation of the volumes B. The fiber vectors $\boldsymbol{n}$ within B are used to determine the local fiber orientation of the individual laminate layers. Since R is sufficiently small, the fiber architecture within B is assumed to be planar.

2.5. Segmentation of laminate layers

The goal of the segmentation is to separate the individual layers within B. As a result, the layer fiber orientations are individually analyzed. Subset L_j of B is defined as volume only containing fibers of layer number j.

$$L_j \subseteq B, \quad \forall j = 1 \ldots m \quad m : \text{Number of layers} \tag{4}$$

Since radius R is small, the layers are planar within B and segmentation is done per voxel slices in $\boldsymbol{e}'_z$-direction. Due to that, the segmentation is reduced to a one-dimensional problem. The general segmentation process is schematically shown in Fig. 3. In this contribution, three different methods for segmentation of the laminate layers are introduced.

2.5.1. The uniform thickness segmentation method (UTS)

Assuming that after the forming process the thickness of the individual laminate layers is still equal, one segmentation approach is given by partitioning B into volumes L_j with equal height. The layer thickness h is then calculated by dividing the total height h_{total} of B by the number of laminate layers m

$$h = \frac{h_{\text{total}}}{m}. \tag{5}$$

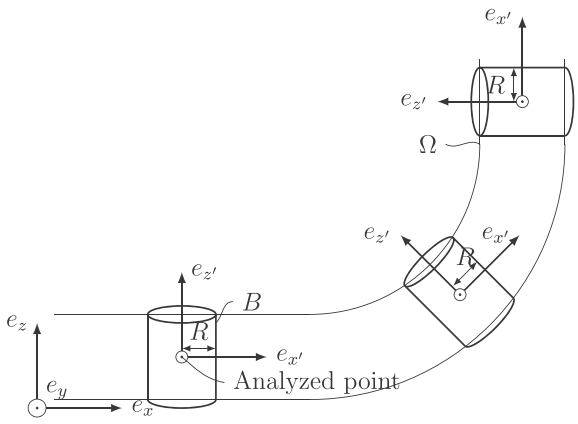

Fig. 2. Alignment of the cylindrical volume B.

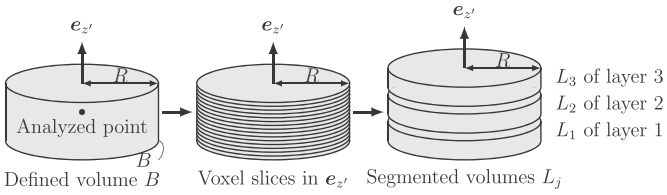

Fig. 3. The principal segmentation process of volume B.

The procedure of this approach is illustrated on a principal sketch with three laminate layers in Fig. 4.

2.5.2. The orientation angle segmentation method (OAS)

Usually, the individual laminate layers are oriented in different directions. Hence, there is a significant change in orientation between adjacent layers. The orientation-angle-segmentation method (OAS)

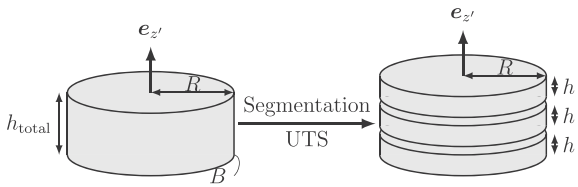

Fig. 4. Schematic illustration of the segmentation method by assuming uniform thickness h (UTS).

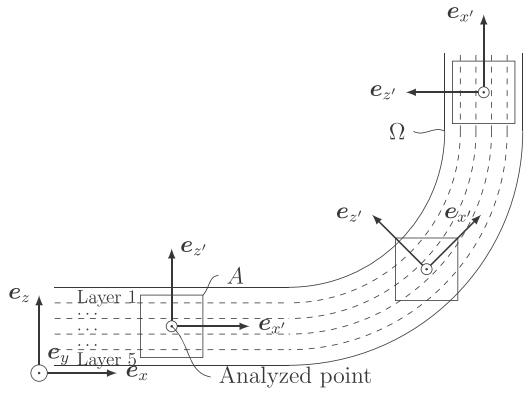

(a) The volume A is defined as a local representative volume around each analyzed point.

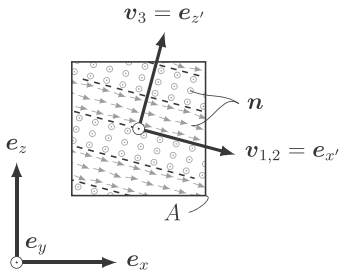

(b) The shell normal direction $\boldsymbol{e}_{z'}$ is orthogonally aligned to the fiber vectors $\boldsymbol{n}$ within volume A.

Fig. 1. Alignment of the local coordinate systems $\{\boldsymbol{e}_{x'}, \boldsymbol{e}_{y'}, \boldsymbol{e}_{z'}\}$.

makes uses of this characteristic change to segment adjacent laminate layers. The second-order orientation tensor $\boldsymbol{N}$ and the corresponding first eigenvector $\boldsymbol{v}_1$, indicating the most significant fiber orientation, are calculated for each voxel slice in $\boldsymbol{e}_{z'}$ direction. The orientation angle φ between $\boldsymbol{e}_{x'}$ and $\boldsymbol{v}_1$ around $\boldsymbol{e}_{z'}$ is defined as a scalar value of the voxel slice fiber orientation (cf. Fig. 5).

The value of $\varphi(z')$ reveals the most significant fiber orientation within a voxel layer and thus changes rapidly from layer to layer. Using the midpoint rule, the numerical gradient of the orientation angle in $\boldsymbol{e}_{z'}$ direction for voxel slice z'_i is determined by

$$\frac{\partial \varphi}{\partial z'}(z'_i) \approx \frac{\varphi(z'_{i+1}) - \varphi(z'_{i-1})}{z'_{i+1} - z'_{i-1}}. \tag{6}$$

Inside a laminate layer, φ is almost constant and the gradient $|\partial\varphi / \partial z'|$ is about zero. Between two adjacent layers, φ is changing rapidly, resulting in a $|\partial\varphi / \partial z'|$ peak. Combined with a threshold k, the laminate layers are separated based on those peaks. The threshold k is adjusted adaptively, beginning from a high start value decreasing stepwise until prescribed numbers of m laminate layers are segmented. Fig. 6 schematically demonstrates the OAS method.

2.5.3. The coherence minima segmentation method (CMS)

Assuming that the radius R of B is sufficiently small, fibers within the same (unidirectional-)laminate layer are aligned in the same direction. As a result, the coherence value c_w of a voxel slice within a laminate layer is approximately one. The area between two adjacent layers is introduced as transition zones. Within a transition zone, the fibers of both adjacent layers are located (cf. Fig. 7). Consequently, the coherence value c_w within such a transition zone becomes small. As a result, the coherence value c_w distribution along $\boldsymbol{e}_{z'}$ direction indicates a local maximum within a laminate layer and a local minimum between two laminate layers. Based on those coherence minimums, the laminate layers within B are segmented. The illustration in Fig. 8 schematically shows the segmentation based on the coherence minimums.

Since the coherence value c_w is sensitive, image noise is a big challenge while determining those coherence minimums. To eliminate minimums caused by noise, the coherence signal is smoothed by filters, for example the median or sigma filter [22–25]. To apply proper filter parameters, the filter parameters are adjusted adaptively and individually for each analyzed point, by increasing the filter parameter stepwise until m laminate layers are segmented. Due to the minima of c_W caused by image noise, the criterion for a minimum is enhanced in such a way, that $c_{w,i}$ has to fulfill

$$c_{w,i-2} > c_{w,i-1} > c_{w,i} < c_{w,i+1} < c_{w,i+2}. \tag{7}$$

2.6. Mapping process

The segmentation methods presented in Section 2.5, segment the laminate layers within B and return volumes $L_j \quad j = 1, \ldots, m$. The volumes L_j only containing fiber vectors $\boldsymbol{n}$ of the corresponding laminate layer j. The mapping methods determines the local fiber orientation of the individual laminated layers and maps the result to a FE mesh. Based on the fiber vectors $\boldsymbol{n}$ within L_j, the second-order orientation tensor and related eigenvectors for each laminate layer are determined. As introduced, the first eigenvector $\boldsymbol{v}_1$ represents the most relevant fiber orientation and thus, is returned as the resulting local fiber orientation of the

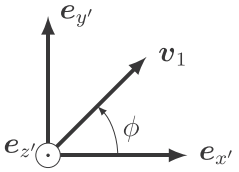

Fig. 5. Definition of the orientation angle φ.

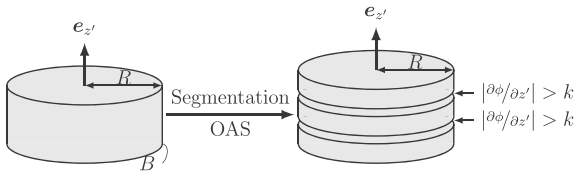

Fig. 6. Illustration of the segmentation method by using the orientation angle φ change (OAS).

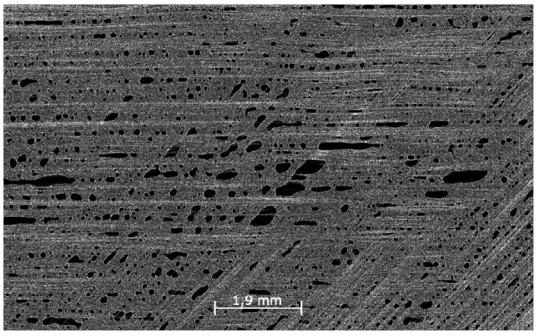

Fig. 7. Exemplary gray value image of a voxel slice within a transition zone of a quasi-isotropic carbon fiber-reinforced PA6 sample. Isotropic voxel spacing: 0.0095 mm.

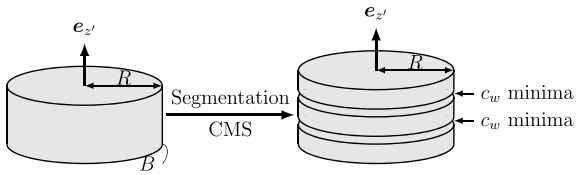

Fig. 8. Illustration of the segmentation method by using the minimums of the coherence c_w.

corresponding laminate layer. Three mapping methods with different mapping strategies are presented in this manuscript.

2.6.1. Arithmetic weight mapping (AWM)

The Arithmetic Weight Mapping (AWM) approach is given by taking all N fiber vectors $\boldsymbol{n}$ within the segmented volume L_j and weight them by a uniform factor:

$$\boldsymbol{N}_j = \frac{1}{N} \sum_{\boldsymbol{n}_i \in L_j} \boldsymbol{n}_i \otimes \boldsymbol{n}_i. \tag{8}$$

2.6.2. The centric voxel slice selection mapping (CVM)

Transition zones contain fibers of both adjacent layers (cf. Fig. 7). The segmented volumes L_j can still contain parts of these transition zones, which can result in distortedly mapped laminate layer fiber orientations. To avoid that, a pre-selection is implemented to sort fiber vectors of the transition zones within L_j out. The centric voxel slice selection mapping approach (CVM) only takes fiber vectors located within the centered voxel slice into account for calculating $\boldsymbol{N}$. The location of the centric voxel slice is visualized in Fig. 9. Consequently, the selected fiber vectors are most distanced to both transition areas. The centric voxel slice $M_j \subset L_j$ is defined as the voxel slice in the middle of L_j with respect to $\boldsymbol{e}_{z'}$ (cf. Fig. 9). The second-order orientation tensor is calculated by

$$\boldsymbol{N}_j = \frac{1}{N} \sum_{\boldsymbol{n}_i \in M_j} \boldsymbol{n}_i \otimes \boldsymbol{n}_i. \tag{9}$$

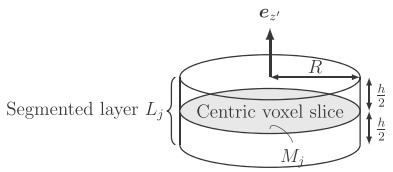

Fig. 9. Mapping method by selecting the centric voxel slice.

2.6.3. The anisotropic Gaussian function mapping (AGM)

Another way to avoid distorting effects by the transition zones is to add weighting factors. Distorting transition zones are located at the top and bottom of the segmented volume L_j. Therefore they are widely distanced to the center point of L_j. By using a distance-based weighting factor, the fiber vectors within the transition zone are less weighted and the distorting effect is reduced. In the present approach, the weighting factors c are based on the anisotropic Gaussian function. The position of the center point is given by (x_m, y_m, z_m) and the position of voxel i is given by (x_i, y_i, z_i), both related to the local coordinate system $\{\boldsymbol{e}_{x'}, \boldsymbol{e}_{y'}, \boldsymbol{e}_{z'}\}$. By adjusting the parameter $\sigma_{xy} = R/3$ and $\sigma_z = h/3$ the weighting factors c_i are directly coupled to the size of L_j by

$$c_i = e^{-\frac{(x_i-x_m)^2+(y_i-y_m)^2}{2\sigma_{xy}^2} - \frac{(z_i-z_m)^2}{2\sigma_z^2}} = e^{-\frac{d_{xy,i}^2}{2\sigma_{xy}^2} - \frac{d_{z,i}^2}{2\sigma_z^2}}. \tag{10}$$

The second-order orientation tensor $\boldsymbol{N}$ is determined by

$$\boldsymbol{N}_j = \frac{1}{\sum c_i} \sum_{\boldsymbol{n}_i \in L_j} c_i \boldsymbol{n}_i \otimes \boldsymbol{n}_i. \tag{11}$$

3. Validation

3.1. Material and laminate layup

The relevant segmentation and mapping method combinations are applied on planar samples of unidirectional carbon fiber-reinforced PA6 tape (UD-tape) laminates (cf. Table 1). The samples used for the validation are only stacked and pre-consolidated to rectangle plates, without thermoforming into a 3-dimensional geometry. As a result, the initial fiber orientation is not changed due to the missing forming process step. The stacked laminate layers are aligned in $[90°, 45°, 0°, -45°, -45°, 0°, 45°, 90°]$ direction (quasi-isotropic stacking sequence, QI). The sample consists of eight layers, but fibers in layer number four and five are aligned in the same direction (double layer). The samples are cut out by water jet.

3.2. Experimental image generation and validation procedure

Volumetric images are acquired by a YXLON-Computed-Tomography-System with a PerkinElmer detector (detailed parameter are listed in Table 2). To reconstruct the finale volumetric image, the Feldkamp algorithm [26] is applied. The resulting image voxel spacing is 9.5 µm per voxel. Subsequently, fiber orientation vectors $\boldsymbol{n}$ are determined by using the orientation analysis method based on the structure tensor [6,12].

A mesh of 24 triangle elements and one Gaussian point in each element center is defined. Volume B is defined by a cylinder with radius $R = 50$ voxel($= 0,475$ mm).

The essential steps of the presented approach are mapping and segmentation. Mapping is an important step, but for successful execution proper segmentation is essential. Thus, the validation focuses on the three presented segmentation methods. Due to its the robustness, the AGM method in Section 2.6.3 is selected to perform the mapping step.

For validation of the applied methods, the resulting fiber orientations are compared to representative gray value images. The validation results for the laminate layer number one to three are exemplary shown.

3.3. Validation of uniform thickness segmentation

The cylindrical volumes B are partitioned by using the UTS method in Section 2.5.1. The UTS method takes only the total height of B into account and assumes that all laminate layers have the same height h. Resulting fiber orientations are presented in Fig. 10 together with representative gray value image of the related laminate layers (image of voxel slice at $z' = 7$, $z' = 19$, and $z' = 31$).

3.4. Validation of orientation angle φ segmentation

The volumes B are partitioned into segmented volumes L_j by using the OAS method introduced in Section 2.5.2. Fig. 11 shows the resulting orientations of the first three laminate plies and the corresponding representative gray value images (image of voxel slice at $z' = 7$, $z' = 19$, and $z' = 31$).

In Fig. 12 (a) the orientation angle φ of the fiber vectors within B, (b) the distribution of the orientation angle gradient and (c) the orientation angle are shown for an exemplary Gaussian point. There are seven laminate plies with different fiber orientations segmented. Six peaks between neighboring laminate layers are detected. The green bar shows the final adapted threshold k. The red points mark the top and bottom of the segmented volume L_j. The voxel slices, which are on the right-hand side of the green bar do not meet up the condition $\left|\frac{\partial\varphi}{\partial z'}\right| < k$ and hence are not assigned to any L_j.

The OAS method detects the layer number four and five as a single layer with double-size thickness (cf. Fig. 12 (a)–(c)). In Fig. 12 (b) the illustrated gradient $|\partial\varphi / \partial z'|$ only shows smalls peaks within the double layer (layer no. 4, $z' = 37 \ldots 61$). The fibers within these two layers are aligned in the same direction and therefore, no significant change in the orientation angle distribution exists.

3.5. Validation of coherence c_w segmentation

The local volumes B are segmented by applying the CMS method, introduced in Section 2.5.3. In Fig. 13, the resulting fiber orientations of layer number one, two and three are presented together with representative gray value images of these plies (image of voxel slice at $z' = 7$, $z' = 19$, and $z' = 31$).

In Fig. 14 (a) the fiber architecture within B is illustrated by a surface

Table 1
Properties of the applied material.

Name	Parameter
Trade name	BASF Ultratape B3EC12 UD02 0160
Matrix	Polyamide 6
Fiber	Carbon
Reinforcement type	Unidirectional
Fiber volume content	49.0 %
Density	1.46×10^3 kg/m^3
Tape thickness	0.16 mm

Table 2
Parameters of the CT scans.

Name	Parameter
CT-System	YXLON-CT-System
Detector	Perkin Elmer Y.XRD1620 (2048 × 2048 pixels)
Acceleration voltage	110 kV
Current	0.18 mA
Exposure/Integration time	500 m s
Reconstruction algorithm	Feldkamp [26]

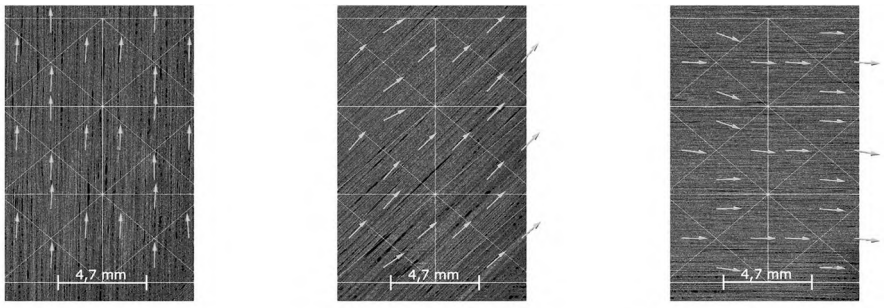

(a) Layer one, $z' = 7$ (b) Layer two, $z' = 19$ (c) Layer three, $z' = 31$

Fig. 10. Determined fiber orientations and according gray value images of the related laminate layers. Isotropic voxel spacing: 9.5 µm. Segmentation: UTS, Mapping: AGM, Radius $R = 50$ voxel $= 0,475$ mm.

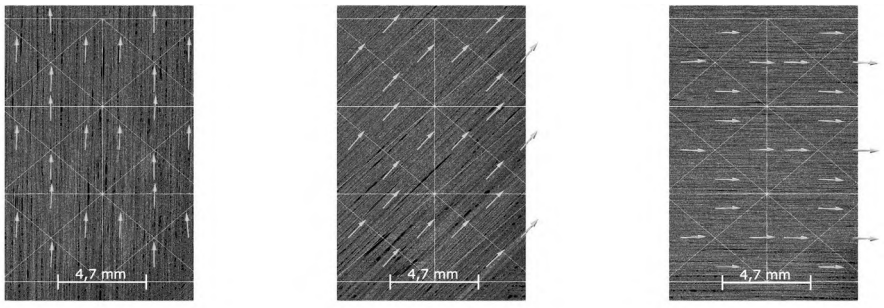

(a) Layer one, $z' = 7$ (b) Layer two, $z' = 19$ (c) Layer three, $z' = 31$

Fig. 11. Determined fiber orientations and according gray value images of the related laminate layers. Isotropic voxel spacing: 9.5 µm. Segmentation: OAS, Mapping: AGM, Radius $R = 50$ voxel $= 0,475$ mm.

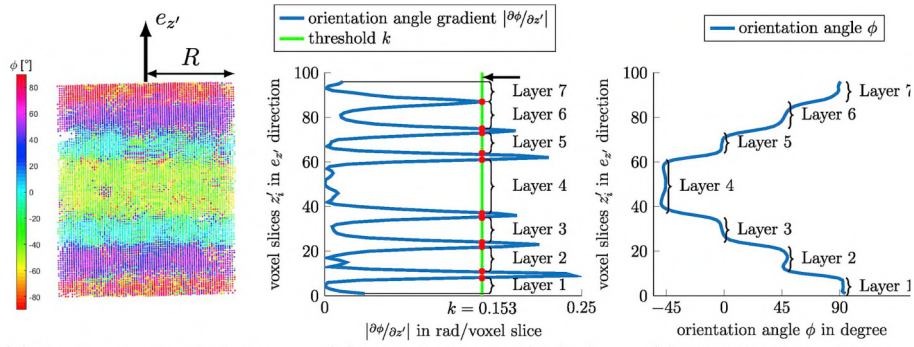

(a) Surface view of B illustrating fiber vector's ϕ (b) Distribution of $|\partial\phi/\partial z'|$ along $\boldsymbol{e}_{z'}$ (c) Distribution of fiber vector's ϕ along $\boldsymbol{e}_{z'}$

Fig. 12. Segmentation of laminate layers based on $|\partial\varphi\,/\partial z'|$ and an adaptive threshold k.

view of the fiber vectors orientation angles φ. In order to sort out minima caused by noise, the median filter is applied. The original and the final coherence c_w distribution of a representative Gaussian point are respectively plotted in Fig. 14 (b) and (c).

The analyzed specimen consists of eight plies, although fibers in laminate layer number four and five are aligned in the same direction. In contrast to the OAS method, double-size layers are separated by the CMS method (cf. minima at $z'_i = 50$ in Fig. 14 (c)). Inside the transition zone between two laminate layers with the same orientation, pores and matrix enrichments are mainly responsible for the detected coherence minimum. A gray value image of a transition zone is shown in Fig. 15.

3.6. Performance comparison

Since the performance of image processing methods is important for practical application, the performance of all three segmentation methods is compared based on a benchmark test. For benchmark testing, the segmentation methods determine the UD-FRP laminate layer fiber orientation of six different samples. All six benchmark samples consist of eight UD-FRP layers and for each sample the local fiber orientation is analyzed at 144 points. The resulting mean computational times and comparative values are listed in Table 3. All benchmark test were performed on a computing system with two Intel® Xeon® CPU X5680 processor units and 96GB of RAM.

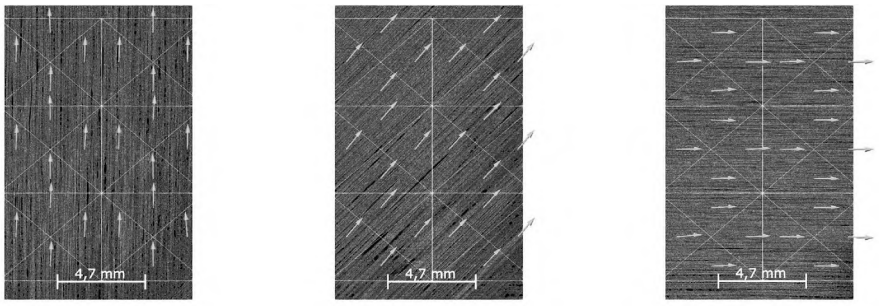

(a) Layer one, $z' = 7$. (b) layer two, $z' = 19$. (c) Layer three, $z' = 31$.

Fig. 13. Determined fiber orientations and according gray value images of related laminate layers. Isotropic voxel spacing: 9.5 µm. Segmentation: CMS, Mapping: AGM, radius $R = 50$ voxel $= 0,475$ mm.

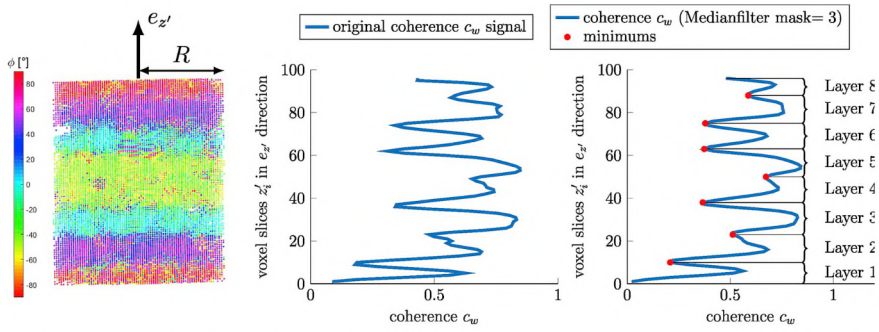

(a) ϕ of fiber vectors within B (b) original c_w distribution (c) smoothed c_w distribution

Fig. 14. Segmentation of the laminate layers based on the minimums of the coherence c_w distribution.

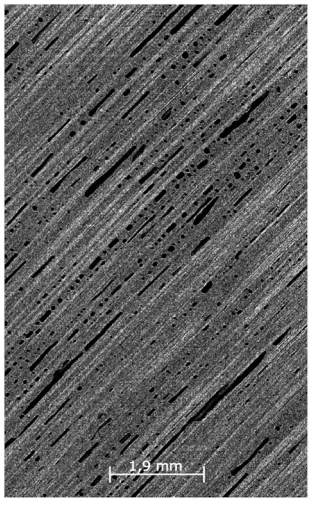

Fig. 15. Image slice within the transition zone between layer four and five of the analyzed quasi-isotropic sample. Isotropic voxel spacing: 9.5 µm. Carbon fiber-reinforced PA6.

Table 3
Benchmark test results of the segmentation methods based on six UD-FRP samples with each 144 analyzed points and eight layers.

Method	Mean CPU time	Comparative value
UTS	17 min3 sec	100% (reference)
OAS	26 min22 sec	155%
CMS	28 min16 sec	165%

4. Application to a generic geometry

4.1. Example component and application procedure

During the forming process step, the fiber orientation of UD-laminate components is changing significantly. Since the fiber orientation has a fundamental impact on the mechanical properties, reliable numerical models to determine the fiber orientation within the final component are needed. The presented approaches can be used to characterize the local fiber orientation of the individual layers. The acquired data can be used to validate numerical process simulation models. An exemplary generic geometry is illustrated in Fig. 16, [27]. The laminate layers are initially aligned in $[90°, 45°, 0°, -45°, -45°, 0°, 45°, 90°]$ direction (same stacking sequence as the sample in Section 3). The generic component is made of the same material as the samples in Section 3 (cf. Table 1). The presented methods are applied to determine the local fiber orientation within two exemplary samples of the final component. The samples are cut by water jet. Local fiber orientations of both samples are analyzed on the Gaussian points of a finite element mesh and determined by the combination of the OAS and the AGM method for segmentation and mapping, respectively. The cylinder radius R is adjusted adaptively. The analyzed volumetric images were generated on a YXLON-System. The volumetric images are acquired in the same manner to those in Section 3 (cf. Table 2). In order to scan the whole lean sample (position 1), the vertical detector enlargement of the CT-System was applied.

Resulting fiber orientation data is determined on the Gaussian points and exported by the neutral VTK-Format. The fiber orientations obtained by the presented volumetric image analysis approach can be compared directly to the results of the process simulation. Moreover, the determined fiber orientations can be used to characterize draping phenomena like folds and wave patterns.

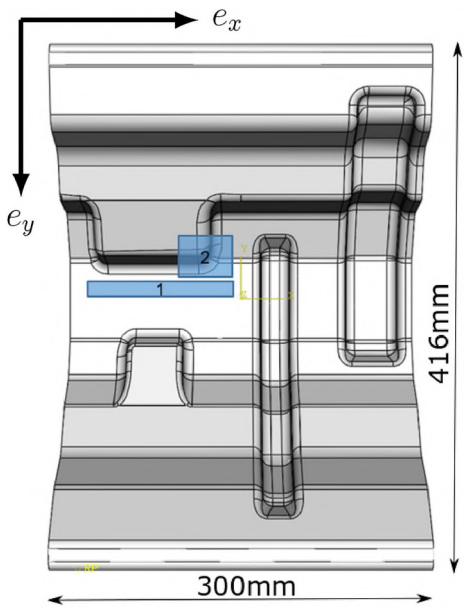

Fig. 16. Generic geometry [27] and position of the extracted specimens.

4.2. Results

The planar sample number one (length: 150 mm, width: 15 mm and thickness: 1.2 mm) is located between two beads (position 1 in Fig. 16). The calculated fiber orientations are presented in Fig. 17. Different kinds of fiber draping phenomena within the individual laminate layers can be observed. Especially within layer number three, where the fibers are aligned parallel to the beads. The determined fiber orientations within layer number one and two show a wave-like pattern.

In complex shaped components a lot of worth knowing fiber phenomena occur. The curved sample number two is located at the double-curved corner of the bead (position 2 in Fig. 16). In order to determine the local fiber orientation within the curved samples, the presented approach (OAS and AGM) is applied. In Fig. 18 the determined fiber orientations of the first four laminate layers are illustrated. Results of layer number one, three and four show, that the fibers are aligned around the corner in this area. In layer number two a fold-like fiber pattern is observed at the top of the corner.

5. Discussion

The segmentation step, separating the individual laminate layers, is the essential step in the presented method and therefore, the validation in Section 3 is focused on the three presented segmentation approaches. According to the comparison of the determined fiber orientations and the representative gray value images in Figs. 11 and 13, both the OAS and the CMS method in combination with the mapping method AGM reliably segment the unidirectional laminate layers and determine accurately the local fiber orientation. Moreover, the CMS method is able to segment adjoining layers with the same fiber orientation (double-size layers). The eigenvalues of the second-order fiber orientation tensor $\boldsymbol{N}$ and the coherence value c_w are sensitive to local imperfections and image noise. This makes it necessary to applying filters. The filter parameters are adaptively adjusted in order to smooth out local coherence minima induced by noise and so only minima caused by layer transition remain. The orientation angle φ, as well as the numerical gradient $\partial\varphi/\partial z$' are hardly affected by image noise and filters do not have to be applied for the OAS segmentation method. According to the benchmark test results in Table 3, the OAS method is more computational efficient than the CMS approach.

Compared to the results of the OAS and the CMS method, the

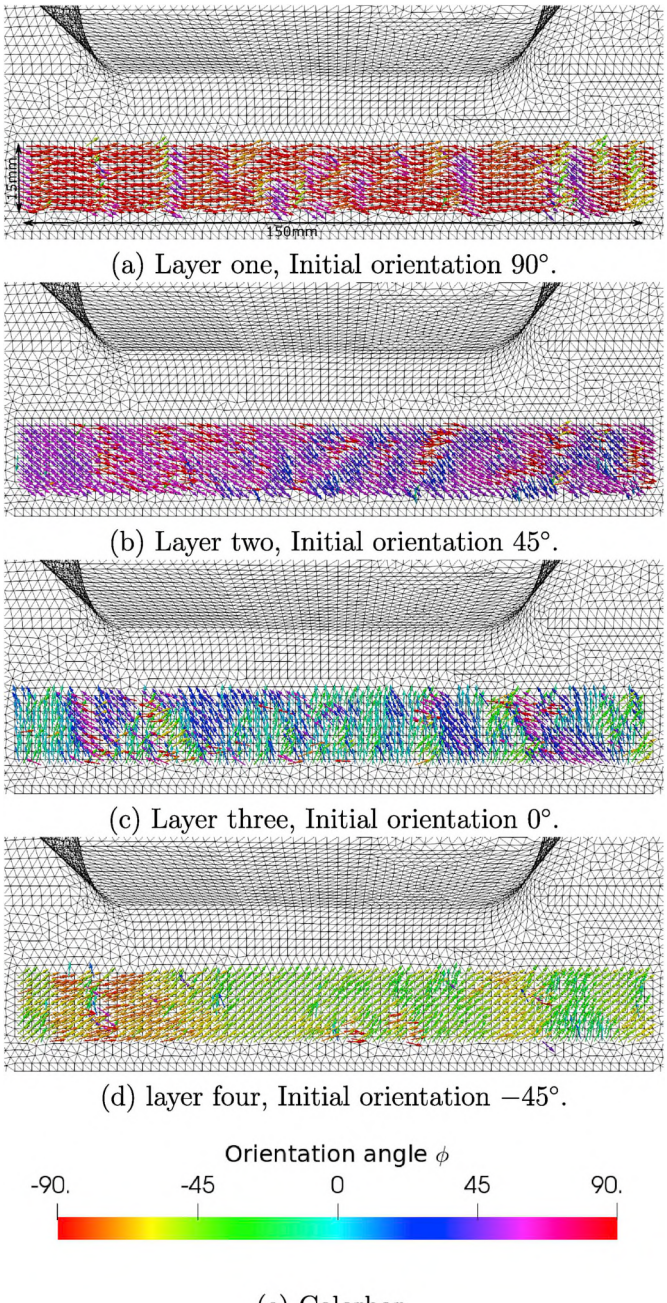

Fig. 17. Determined fiber orientation of the plane QI-sample at position 1. Isotropic voxel spacing: 14.8 µm. Segmentation: OAS, Mapping: AGM, adaptive radius $R \in \{50\ \text{voxel}\ldots20\ \text{voxel}\} = \{0.74\ \mu\text{m}\ldots0.296\ \text{mm}\}$.

determined fiber orientations using the UTS are less corresponding to the fibers in the representative gray value images. Due to the difference between assumed uniform thickness h and the height of the actual layers, segmentation is less accurate and neighbored layers are mixed up. This error in layer height is accumulating from the edge to the core region, which makes this method unusable for analyzing laminates with a large number of layers.

In Section 4 the laminate layer fiber orientation of a generic geometry is determined. Due to resistant against noise, the OAS in combination with the AGM mapping method are selected. The application demonstrates the practical applicability of the presented approach for complex formed UD laminate components.

In this paper, the focus is laid on presenting the analyzing tools and

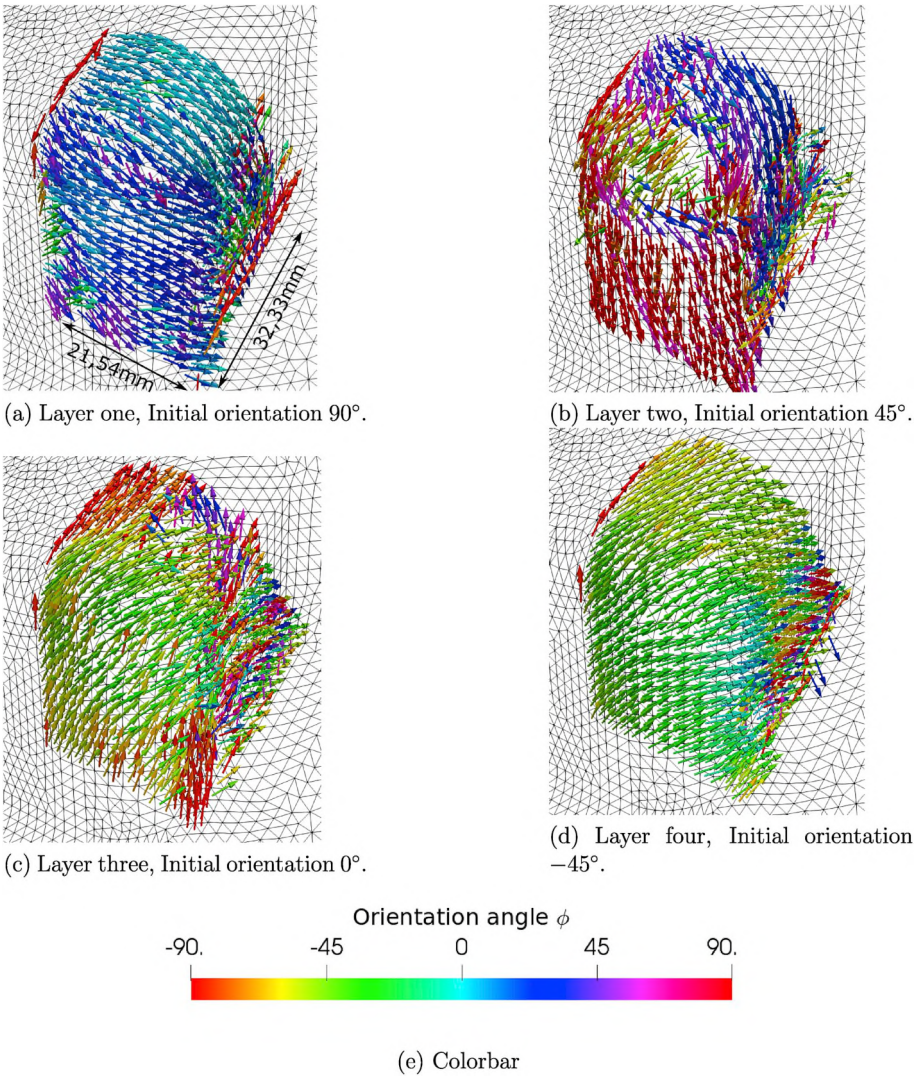

(a) Layer one, Initial orientation 90°.

(b) Layer two, Initial orientation 45°.

(c) Layer three, Initial orientation 0°.

(d) Layer four, Initial orientation −45°.

(e) Colorbar

Fig. 18. Determined fiber orientations of the curved QI-sample at position 2. Isotropic voxel spacing: 25.1 µm. Segmentation: OAS, Mapping: AGM, adaptive radius $R \in \{40 \text{ voxel} \ldots 20 \text{ voxel}\} = \{1.004 \text{ mm} \ldots 0.502 \text{ mm}\}$.

their capability for real part applications. Discussing the observed phenomena in detail is not part of this manuscript. In the contribution of Nguyen et al. [9], mid-layer volumes of each laminate layer is selected manually. In contrast, the introduced approach separates unidirectional laminate layers automatically. Moreover, besides planar also curved shell-shaped specimen are analyzed applying the presented approach. Emerson et al. [7] segmented and characterized individual fibers of unidirectional composites. They scanned a specimen of size 3 mm × 10 mm × 12 mm. The presented approach in this manuscript are applied to 1.2 mm × 15 mm × 150 mm.

6. Conclusion

The presented paper introduces an approach for determining local fiber orientation of continuous fiber-reinforced laminate composites based on volumetric images acquired by x-ray computed tomography. The approach consists of three parts. First the local thickness direction that is orthogonal to the local laminate layers is calculated at specific analyzed points. Based on that a cylindrical volume around that point is defined and the individual laminate layers inside are segmented. Finally, the local fiber orientations of the segmented laminate layers are determined at mapped to a FE mesh.

An essential step of the presented approach is the segmentation of the individual laminate layers. Three segmentation methods are introduced, using the change in orientation angle (OAS method), the minima of the coherence distribution (CMS method) and uniform thickness (UTS method). For mapping of the resulting fiber orientation, it is important to prevent distorting influences of the transition zones. Mapping methods based on a pre-selection filter and distance based weighting factors are presented.

Since laminate layer segmentation is the important step of the introduced approach, the validation is focused on the presented segmentation methods (UTS, OAS and CMS). For validation, samples with known fiber orientation are analyzed and the obtained results are compared to the corresponding gray value images. The validation results demonstrate, that both the OAS and the CMS method reliably segment the individual laminate layers. In addition, the CMS method is able to segment adjoining layers with the same fiber orientation (double-size layers). However, the OAS approach is more robust against noise in contrast to the CMS method. As a result, the CMS method is preferred for segmenting unidirectional FRP laminates with double-size layers and otherwise the OAS method. The UTS method is not as accurate as the other two segmentation methods. Especially, for analyzing laminates with large number of layers.

Finally, a typical application on a generic geometry is presented. The laminate layer fiber orientation of both planar and curved samples is

determined.

Microstructure data are important to develop new numerical material models and process simulation methods. Based on the present approach, the local fiber orientation of each laminate layer are determined and resulting can be used for validation or input data of numerical simulations.

Volumetric images require a lot of memory storage. By determining the local fiber orientation of the individual layers, the essential information is extract from the volumetric images and the required memory storage is reduced.

Authors contribution

Ludwig Schöttl developed, implemented and applied the methods presented in this paper during his master thesis. He also wrote the first draft of the paper. Dominik Dörr initiated the work, supported the method development and the analysis of results. The tool for determining the local fiber orientation on the voxel level based on volumetric gray value images was contributed by Pascal Pinter. Kay André Weidenmann, Peter Elsner (experimental part) and Luise Kärger (numerical part) supervised and coordinated the master thesis of Ludwig Schöttl. Dominik Dörr, Pascal Pinter, Kay André Weidenmann, Peter Elsner and Luise Kärger thoroughly revised the paper.

Acknowledgements

The authors would like to thank the German Federal Ministry of Education and Research for the funding of the project SMiLE (03X3041P), for which the presented work was carried out. Furthermore, the authors acknowledge the partial support by the German Research Foundation (DFG) within the International Research Training Group "Integrated engineering of continuous-discontinuous long fiber reinforced polymer structures" (GRK 2078). As well the authors grateful appreciate the support of Fraunhofer ICT by supplying the experimental forming results of the generic geometry, which were finished under the project leadership of Tobias Joppich.

Nomenclature

$\boldsymbol{N}$	second-order orientation tensor
$\boldsymbol{n}$	fiber orientation vector
$\boldsymbol{v}$	eigenvectors
λ	eigenvalues
φ	orientation angle
ψ	distribution function
σ	Gaussian parameter
$\{\boldsymbol{e}_x, \boldsymbol{e}_y, \boldsymbol{e}_z\}$	global coordinate system
$\{\boldsymbol{e}_{x'}, \boldsymbol{e}_{y'}, \boldsymbol{e}_{z'}\}$	local coordinate system
$\{x_i, y_i, z_i\}$	position of voxel i
$\{x_m, y_m, z_m\}$	center position of L_j
A	considered volume to determine the normal vector
B	considered volume for orientation analysis
c	weighting factors
c_w	coherence of $\boldsymbol{N}$
h	height of L
h_{total}	total height of B
i	voxel (slice) number index
j	layer number index
k	threshold
L_j	segmented volume of layer j
m	number of layers
M_j	centric voxel slice subset of L_j
R	cylinder radius of B
z'_i	voxel slice index in $\boldsymbol{e}_{z'}$ direction

Appendix A. Supplementary data

Supplementary data to this article can be found online at https://doi.org/10.1016/j.ndteint.2019.102194.

References

[1] Eyerer P, Hirth T, Elsner P. Polymer engineering. Springer; 2008.
[2] Jones RM. Mechanics of composite materials. Taylor & Francis; 1999.
[3] Carmignato S, Dewulf W, Leach R. Industrial X-ray computed tomography. Springer; 2018.
[4] Pinter P. *Microstructure Characterization of continuous-discontinuous fibre reinforced Polymers based on volumetric images*. PhD thesis. Karlsruhe Institute of Technology; 2018.
[5] Teuwsen J, Bittner F, Steffen J. Evaluation of x-ray target materials to improve ct-based measurement of fiber orientations inside cf-smc components. In: International symposium on digital industrial radiology and computed tomography - DIR2019; 2019.
[6] Pinter P, Dietrich S, Bertram B, Kehrer L, Elsner P, Weidenmann KA. Comparison and error estimation of 3d fibre orientation analysis of computed tomography image data for fibre reinforced composites. NDT E Int 2018;95(26 – 35).
[7] Emerson MJ, Jespersen KM, Dahl AB, Conradsen K, Mikkelsen LP. Individual fibre segmentation from 3d x-ray computed tomography for characterising the fibre orientation in unidirectional composite materials. Compos Appl Sci Manuf 2017; 97:83–92.
[8] Pinter P, Bertram B, Weidenmann KA. A novel method for the determination of fibre length distributions from µct-data. In: 6th conference on industrial computed tomography; 2016.
[9] Nguyen NQ, Mehdikhani M, Straumit I, Gorbatikh L, Lessard L, Lomov SV. Micro-ct measurement of fibre misalignment: application to carbon/epoxy laminates manufactured in autoclave and by vacuum assisted resin transfer moulding. Compos Appl Sci Manuf 2018;104:14–23.

[10] Requena G, Fiedler G, Seiser B, Degischer P, Di Michiel M, Buslaps T. 3d-quantification of the distribution of continuous fibres in unidirectionally reinforced composites. Compos Appl Sci Manuf 2009;40(2):152–63.
[11] Schladitz K, Büter A, Godehardt M, Wirjadi O, Fleckenstein J, Gerster T, Hassler U, Jaschek K, Maisl M, Maisl U, Mohr S, Netzelmann U, Potyra T, Steinhauser MO. Non-destructive characterization of fiber orientation in reinforced smc as input for simulation based design. Compos Struct 2017;160:195–203.
[12] Krause M, Hausherr JM, Burgeth B, Herrmann C, Krenkel W. Determination of the fibre orientation in composites using the structure tensor and local x-ray transform. Springer; 2009.
[13] Nielsen JD, Madsen KH, Puonti O, Siebner HR, Bauer C, Madsen CG, Saturnino GB, Thielscher A. Automatic skull segmentation from mr images for realistic volume conductor models of the head: assessment of the state-of-the-art. Neuroimage 2018;174:587–98.
[14] Huo J, Wu J, Cao J, Wang G. Supervoxel based method for multi-atlas segmentation of brain mr images. Neuroimage 2018;175:201–14.
[15] Fredo ARJ, Abilash RS, Kumar CS. Segmentation and analysis of damages in composite images using multi-level threshold methods and geometrical features. Measurement 2017;100:270–8.
[16] Henning F, Möller E. Handbuch leichtbau. Hanser-Verlag; 2011.
[17] Gunter T, Poliwoda C, Reinhart C, Dierig T. Apparatus and method for examining components comprising laid fiber composite fabrics or woven fiber composite fabrics. 2018. United States Patent 10,139,353.
[18] Advani SG, Tucker CL. The use of tensors to describe and Predict fiber orientation in Short fiber composites. J Rheol 1987;31:751–84.
[19] Kanatani K. Distribution of directional data and fabric tensor. Department of Computer Science, Gunma University; 1984.
[20] Nabiatek J. Modeling of fiber orientation during injection molding process of polymer composites. Polish Society of Composite Materials; 2011.
[21] Jähne B. Spatio-temporal image processing. Springer; 1993.
[22] Chan RH, Ho C, Nikolova M. Salt-and-pepper noise removal by median-type noise detectors and detail-preserving regularization. IEEE Trans Image Process; 2005.
[23] Lee J. Digital image smoothing and the sigma filter. Comput Vis Graph Image Process 1982;24:255–69.
[24] Jähne B. Digitale bildverarbeitung. Springer; 2005.
[25] Tönnies KD. Grundlagen der Bildverarbeitung. Pearson Studium; 2005.
[26] Feldkamp LA, Davis LC, Kress JW. Practical cone-beam algorithm. J Opt Soc Am A 1984;1(6):612–9.
[27] Dörr D, Brymerski W, Ropers S, Leutz D, Joppich T, Kärger L, Henning F. A benchmark study of finite element codes for forming simulation of thermoplastic ud-tapes. Procedia CIRP 2017;(66):101–6.